Hindawi
Geofluids
Volume 2022, Article ID 5423743, 17 pages
https://doi.org/10.1155/2022/5423743

Research Article

Numerical Analysis of Dynamic Evolution Characteristics of a Large Rock Landslide in Tangjiashan

Zhenyu Wang, Gaowei Yue, Haixiao Lin, and Minmin Li

School of Civil Engineering, Henan Polytechnic University, Jiaozuo, 454000 Henan, China

Correspondence should be addressed to Gaowei Yue; mxlygw@126.com

Received 15 September 2022; Revised 19 October 2022; Accepted 14 November 2022; Published 30 November 2022

Academic Editor: Hailing Kong

The study of landslide dynamic characteristics and accumulation patterns is of great significance for the quantitative evaluation of landslide hazards. This paper takes the Tangjiashan landslide as a research case, a real 3D model was established based on high precision DEM data to determinate the terrain characteristics and pre- and postlandslide image data to determinate the shape and size of the sliding body. Particle flow 3D program (PFC3D) is carried out to reappear the complete movement of the Tangjiashan landslide. And the dynamic characteristic factors are monitored and analyzed such as the velocity and displacement of the landslide body. The result shows that the Tangjiashan landslide is a traction-type landslide, which lasts about 37 s in total and can be divided into four stages: destabilization and destruction, collapse and accelerated sliding, high-speed sliding, and deceleration and accumulation. The maximum sliding distance is about 642.05 m and the maximum sliding speed is about 38.67 m/s. This is a typical high-speed short-range landslide, and the speed of sliding body surface is much greater than that of other parts, which show an obvious characteristic of clastic flow. In the Tangjiashan landslide, the slip distance is the controlling factor in determining the speed of the landslide at different locations.

1. Introduction

In nature, a landslide is one of the most common geological hazards and poses a great threat to the safety of human life and property. The study of dynamic evolution characteristics of landslides has great significance for the quantitative and qualitative evaluation of landslide hazards, which provides guidance for disaster prevention and reduction. In recent years, with the rapid development of computer technology, numerical simulation has been widely used in landslide hazard research with its outstanding advantages such as low cost, good repeatability, and easy and flexible parameter setting [1]. Huang et al. [2–5] reproduced the complete motion process of high-speed remote landslides through various simulation methods such as DDA and finite difference method and conducted an in-depth study on the remote sliding mechanism of high-speed remote landslides. Zhao et al. [6] combined simulation and experiment to conduct a comprehensive and systematic study of fluidization, which reveals the disintegration and fragmentation effects during landslide collisions, aerodynamic effects during the high-altitude flight phase, and the high-speed sliding mechanism.

Particle flow Code (PFC) programs have been more widely applied to the study of landslide dynamics problems because of their rich and flexible contact models that can simulate discontinuities such as dislocation and separation of media [7–10]. Lo et al. [11–13] used PFC3D numerical simulation methods to invert the damage and motion processes of rocky landslides and combined with specific geological structures to analyze and explore the landslide damage. Zou et al. [14, 15] reproduced the complete dynamic process of the Jiweishan landslide through the numerical simulation program PFC2D based on field mechanical test tests, and revealed the depositional characteristics and long-distance transport mechanism of the Jiweishan landslide. Zhou et al. [15, 16] inferred two landslides occurring in the gully zone through the PFC3D discrete element program and combined their specific geological conditions to assess the risk of the two landslides.

Chen et al. [17, 18] analyzed the effects of seismic forces with different characteristics on slope damage and landslide movement processes based on examples of seismic landslides, combined with discrete element numerical simulations. Although PFC3D numerical simulation program has been widely used in the study of landslide problems, the traditional 3D terrain modelling method has been criticized for its disadvantages such as cumbersome and complicated operation and uncontrollable accuracy. The author has therefore adopted the Rhino one-stop modelling approach. The terrain surfaces are first generated directly by Rhino's built-in plugin, then transformed into a terrain body consisting of a suitable triangular mesh according to Rhino's basic functions, and finally exported to a format suitable for PFC3D according to Rhino's format conversion function. Scholars have focused their research on landslide hazards on the influence of geological conditions and geological features on landslide movement and accumulation processes, while research on the mechanics and dynamic evolutionary properties of landslides is still relatively scarce.

In this paper, the mechanical and dynamic evolution characteristics of landslides are investigated, and their movement characteristics are quantitatively and qualitatively analyzed. The Tangjiashan landslide, a super-large compliant rocky landslide, is taken as the object, a real three-dimensional model is constructed according to high-precision DEM data and pre- and postlandslide image data. Based on indoor uniaxial experiments of the sliding body lithology, the fine-scale parameters were determined. Using PFC3D numerical simulation software, the complete process of the Tangjiashan landslide was inverted. And through the analysis of characteristic data such as velocity, displacement, trajectory, and morphology of the landslide, the dynamic evolution characteristics of the Tangjiashan landslide were revealed, which provide reference for the study of dynamic characteristics and dynamic processes of similar landslides.

2. Geomorphological and Geological Features

2.1. Topography. The Tangjiashan landslide is located on the right bank of the Tongkou river, approximately 4.5 km upstream of Beichuan County. The Tongkou river is one of the main tributaries of the Fujiang River, and Tangjiashan is located in the middle reaches of the river, where the river is narrow and steep. The upper part of the slope is gentle about 30° and the lower part is steeper about 50°. The top of Tangjiashan is about 1800 m, and the slip source area is about 1270 m, with Dashuiwan on the left of the slip source area, Yijiawan on the upper right, Yuanhe dam on the opposite side. And Loufangping Village on the inner side of Yuanhe dam, where the slope of Yuanhe dam is about 180 m with a gentle slope of about 25° on the upper side and a steeper slope of about 45° on the lower side [19–21]. The geomorphological features of Tangjiashan are shown in Figure 1.

2.2. Stratigraphic Lithology. The Tangjiashan slope can be divided into two layers according to lithology: the upper layer is a strongly to weakly weathered tuff with a thickness of about 8-25 m; the lower layer is fresh, unweathered grey marl with an approximate thickness of 55 m, interspersed with soft and weakly muddied layers. The Tangjiashan landslide source area is divided by rock structure, from the bottom to the top, with intact laminated rock masses, slightly weathered laminated and broken rock masses, and strongly weathered loose body accumulations. The rock structure profile is shown in Figure 2.

2.3. Landslide Characteristics. The Tangjiashan landslide is an earthquake-induced high-speed short-range landslide. When the large earthquake occurred, the leading edge of the landslide body was first damaged, and as the intensity of the earthquake continued to increase, cracks in the leading edge gradually penetrated to both sides, and under the pull of the slide's gravity, cracks also appeared in the upper edge of the slide body, and then the slide body began to slide downwards [14]. Due to the mountain's steepness, the landslide impacted downwards at high speed and then hit the Yuanhe dam on the opposite bank, forming a giant landslide dam. According to the classification of landslide damage form, the Tangjiashan landslide belongs to traction damage landslide; according to the type of geotechnical body of the landslide, the Tangjiashan landslide again belongs to rocky landslide; according to the scale of the landslide body, the Tangjiashan landslide again belongs to giant landslide [23].

2.4. Landslide Source Areas. The landslide source area of the Tangjiashan landslide is located in the north direction of Tangjiashan, with an overall circle and chair shape, of which the central lower part is the widest, the widest is about 550 m, the average width is about 500 m, the length is about 820 m the average length is about 700 m, the estimated area is $3.15 \times 10^5\,m^2$. The central lower part of the landslide source area is the thickest, gradually thinned to the upper and lower sides, the thickest part is about 80 m, the thinnest part is about 20 m, the average thickness is about 57 m, and the estimated volume is about $2 \times 10^6\,m^3$. Most of the source area is slightly weathered marl, with the lower marl containing muddy and weak inclusions and a certain thickness of strongly weathered loose accumulation on the surface.

2.5. Analysis of Landslide Movement Deposition Processes. After the strong earthquake, the slope of Tangjiashan was under the action of seismic force, the lower edge of the slide source area first produced cracks, and then the joint action of seismic force and gravity produced a pulling crack on the upper edge of the slide source area, with the continuous action of seismic force, the cracks became deeper and deeper until the whole penetrated the whole slide source area. After the formation of the through fissure, the slide began to accelerate downwards. Due to the steep alpine slope, the slide accelerated rapidly until the leading edge of the slide squeezed into the foot of the Yuanhe dam, where the acceleration process ended. Under the effect of the huge impact generated by the high-speed collision, a large amount of rock debris flew out, and the front edge of the broken slide continued to impact forward to a certain height before stopping and falling back down to the Tongkou river under the effect

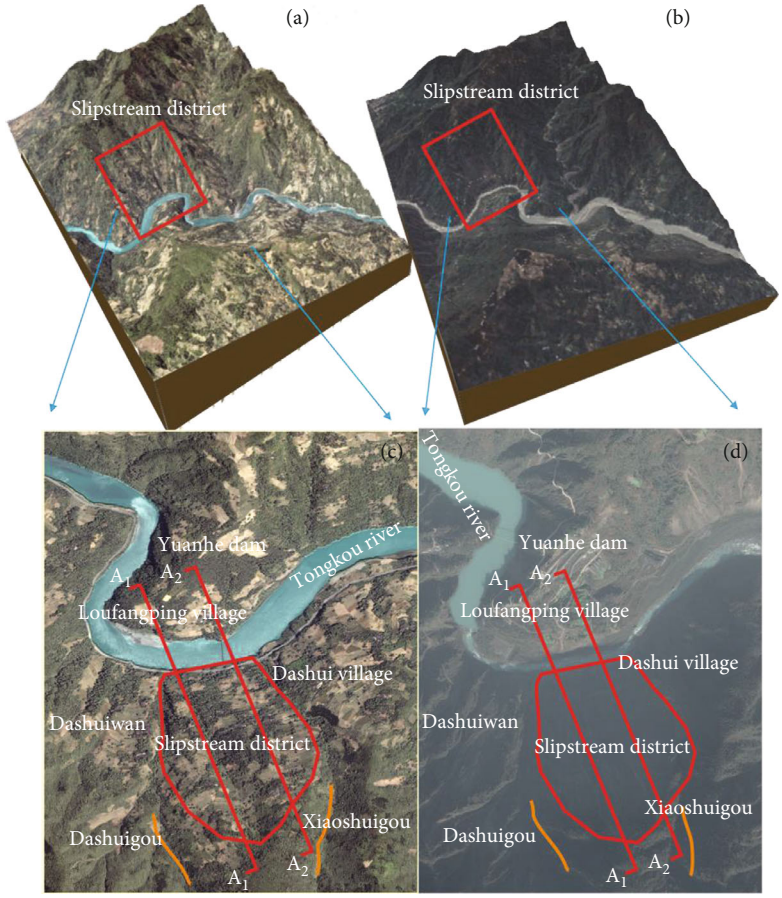

Figure 1: Comparison of the terrain before and after the landslide. (a) General view of the prelandslide terrain. (b) General view of the postlandslide terrain. (c) Enlarged view of the local topography before the landslide. (d) Enlarged view of the local terrain after the landslide.

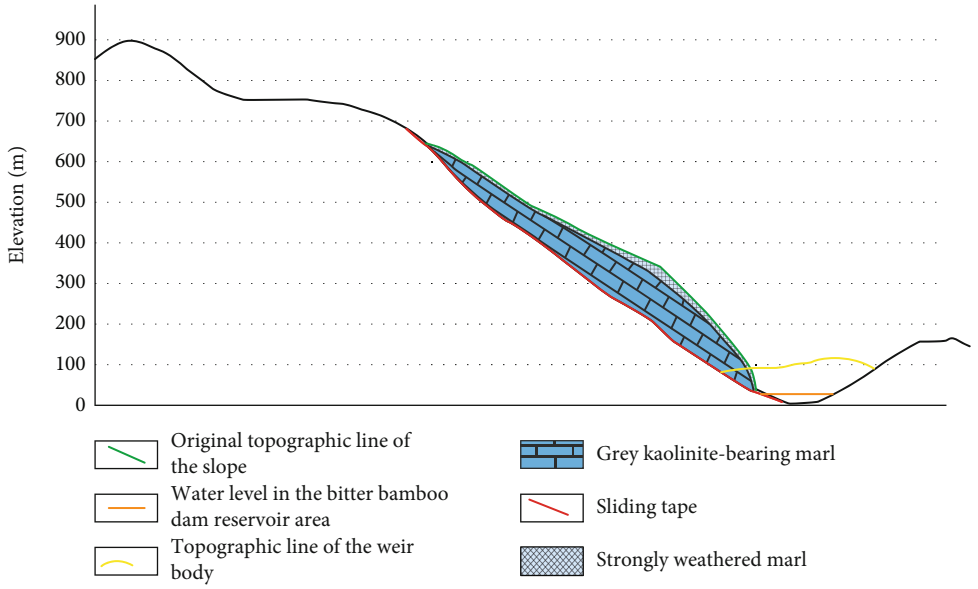

Figure 2: A_1 - A_1 cross-sectional geological profile [22, 23].

of gravity. Due to the narrow river channel and the huge volume of the deposited landslide, the Tongkou river was completely blocked, forming an oversized landslide weir. Combined with the geological terrain conditions at the site, the analysis inferred that the slide body was less damaged in the process of sliding down, except for the bottom, which

caused some rock disintegration due to friction with the terrain, and the rest of the internal structure was less damaged until the slide body impacted the Yuanhe dam. The huge impact destroyed the slide body's rock structure, producing a large amount of debris.

3. Dimensional Model Construction of the Tangjiashan Landslide

3.1. Selection of the Contact Model. Unlike finite elements, which can directly assign macroscopic parameters to a material, PFC (particle flow) requires an intrinsic contact model of the particles to represent the target material's macroscopic physical and mechanical properties. By setting up a reasonable and simple contact model for different models, it is possible to represent the various nonlinear and complex intrinsic properties formed by different combinations of particles. Only by defining the intrinsic contact model can the PFC3D model be used to calculate the mechanical behavior of the particles at the next step and the final physical-mechanical state of the particles, thus reflecting the overall deformation and motion through the constant repetition of the law of force-displacement and Newton's second law.

In granular flows, three intrinsic models are commonly used: the Contact-stiffness model, the slip model, and the bonding model, which describe the elastic relationship between the particles, the sliding process, and the bonding properties, respectively [24]. The stiffness model describes the relationship between force and deformation between the particles, the sliding model describes the relationship between the normal contact force and the tangential force, and the bonding model describes the limits on the magnitude of the normal contact force and the tangential force and the failure of the bond once the bond strength is exceeded. The linear stiffness model, the sliding model, and the parallel bonding model have been chosen for this paper and are formulated as follows.

3.1.1. Linear Stiffness Model. The linear contact stiffness model, one of the most basic models for particle flow, can be applied to most situations. The linear contact stiffness model defines the stiffness between two particles in series, which is defined jointly by the stiffness of particle a and b. Its main parameters are k_n (normal stiffness) and k_s (tangential stiffness) in N/m.

$$k_n = \frac{k_n^a k_n^b}{k_n^a + k_n^b},$$
$$k_s = \frac{k_s^a k_s^b}{k_s^a + k_s^b}. \tag{1}$$

Where ${k_n}^a$ and ${k_n}^b$ are the normal stiffnesses of the two particles a and b in contact, respectively; ${k_s}^a$ and ${k_s}^b$ are the tangential stiffnesses of the two particles a and b in contact, respectively.

3.1.2. Sliding Model. The sliding model, mainly used to describe the relative sliding between particles, specifies the relationship between the tangential and normal forces in contact. Given a defined normal force, sliding between particles occurs when the tangential force exceeds a specific value. The sliding contact model cannot withstand normal tensile forces. The main contact parameter is the coefficient of friction μ, which is the smaller value when the two particles have different coefficients of friction μ. When the overlap between the particles $U^n \le 0$, the contact fails, and both the normal and tangential forces are zero; when $F_{smax} \ge \mu F_n$, the relative sliding between the contacting spheres occurs, neither the normal nor the tangential forces of the contact disappear, and the sliding contact model continues to act. It is worth emphasizing that since the sliding model is point contact, its parametric coefficient of friction μ is not exactly equal to the macroscopic coefficient of friction μ, which is studied face-to-face. The difference is that they are usually of unequal numerical value, and the sliding model often exists in conjunction with other models.

3.1.3. Parallel Bonding Model. The parallel bonding model represents the intrinsic properties of the interlayer or cementing material within the small space where the particles are in contact. When contact is made, it can be imagined that the contacting particles are filled with a certain amount of cement covering them, acting on them with forces and moments. The parallel bond model can be thought of as several springs arranged at the contact, the combined stiffness of which corresponds to the normal and tangential stiffness of the contact model, respectively. The parallel bond model not only resists tensile forces in all directions but also certain bending moments because the contact in the parallel bond contact model is not a point but a surface with a radius of the connect button. When a particle is stressed or tends to move, forces and moments are generated at the contact, but when the sum of these forces or moments, in the tangential or normal direction is greater than either the tangential or normal bond strength, the bond will break.

There are five main parameters of the parallel bond model, namely, bond radius, normal and tangential stiffness, and normal and tangential bond strength. The bond radius controls the properties of the contact surface, the normal and tangential stiffnesses control the deformation of the contact and the normal and tangential bond strengths control the strength of the contact.

3.2. Determination of Fine Physical and Mechanical Parameters of Sliding Body. For numerical simulations of granular flows, the reasonableness of the parameters is directly related to the numerical simulation results. For researchers engaged in engineering research, experiments are the most basic means to determine the parameters of geotechnical bodies [25]. In this paper, the strength parameters of the upper strongly weathered tuff and the lower fresh grey ridge-bearing marl of the slide were determined separately by indoor uniaxial compression tests combined with the Engineering Geology Handbook (China Construction Industry Press, 2018).

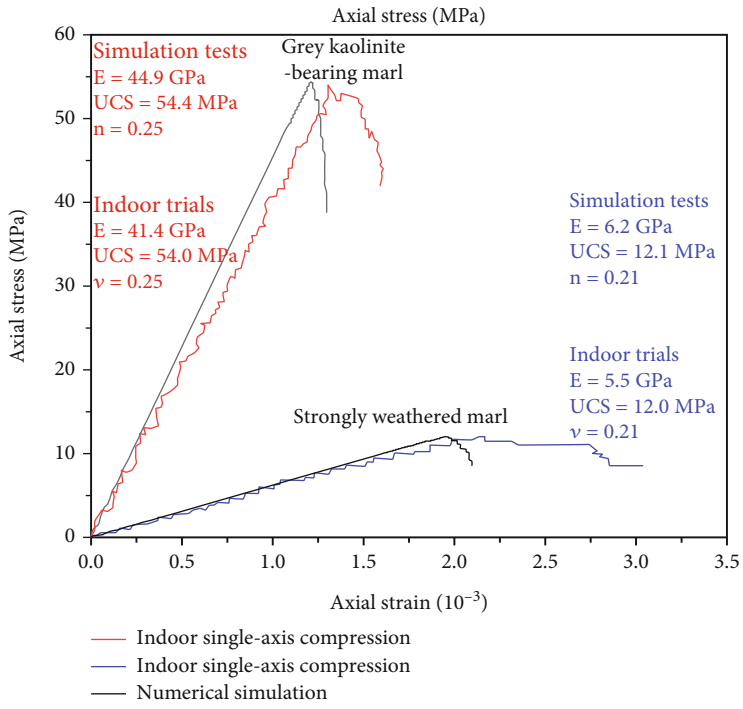

Figure 3: Uniaxial compression test of slip body geotechnical body.

After determining the basic mechanical parameters of the rock, the uniaxial compression test of the simulated rock (Figure 3) was used to repeatedly adjust the fine view parameters by trial and error and combined with the real movement characteristics of the landslide simulation inversion, and a reasonable fine view parameter was finally determined to simulate the Tangjiashan landslide (Table 1), which achieved the basic consistency with the Tangjiashan landslide movement and accumulation process.

3.3. 3D Modelling of Terrain and Sliding Body. PFC simulations of slope problems can usually be divided into two model types, a Ball-Ball model and a Ball-Wall model. The former fills both the slide body and the slide bed with particles, which is suitable for landslides that have not occurred or where the slip surface cannot be determined and can generally be used to predict the landslide damage surface. However, it also has the disadvantages of many particles, low calculation efficiency, difficulty in reasonably determining the particle parameters, and the tendency to produce large errors. The latter distinguishes between a slip bed, which is filled with particles, and a slide bed, which is generated by a wall, and is the ideal rigid body, generally used for landslides that have already occurred or where an obvious slip surface can be identified, with fewer particles, more efficient calculations, and relatively easy to determine parameters [26]. Considering the computer performance and the landslide characteristics, the Ball-Wall model is used in this paper, and the modelling steps are rough as follows.

(1) Firstly, according to the high-precision DEM before and after the landslide, combined with the results of the on-site geological survey, the scope of the landslide source area was determined. Using the 3D modelling software Rhinoceros, the DEM data is converted into a 3D surface, one of which is retained where it overlaps and the lower part is retained where it does not as the landslide bed; the upper and lower parts of the two surfaces that intersect are retained to form a closed surface, which is the model of the landslide source area. Use griddle grid

Table 1: Table of slide detail parameters.

Fine physical parameters of the geotechnical body	Strongly weathered marl	Grey marl with kaolinite
Particle density (g.cm^{-3})	1.90	2.30
Grain size (m)	2.3 ~ 2.7	3.5 ~ 4.0
Normal phase contact stiffness (MPa)	8	20
Tangential contact stiffness (MPa)	8	20
Friction coefficient	0.64	0.89
Normal bond stiffness (MPa.m^{-1})	150	200
Tangential bond stiffness (MPa.m^{-1})	150	200
Bond radius factor	0.4	0.4
Normal bond strength (kPa)	310	910
Tangential bond strength (kPa)	140	510
Local damping	0.05	0.05
Normal critical damping	0.60	0.67
Tangential critical damping	0.60	0.67

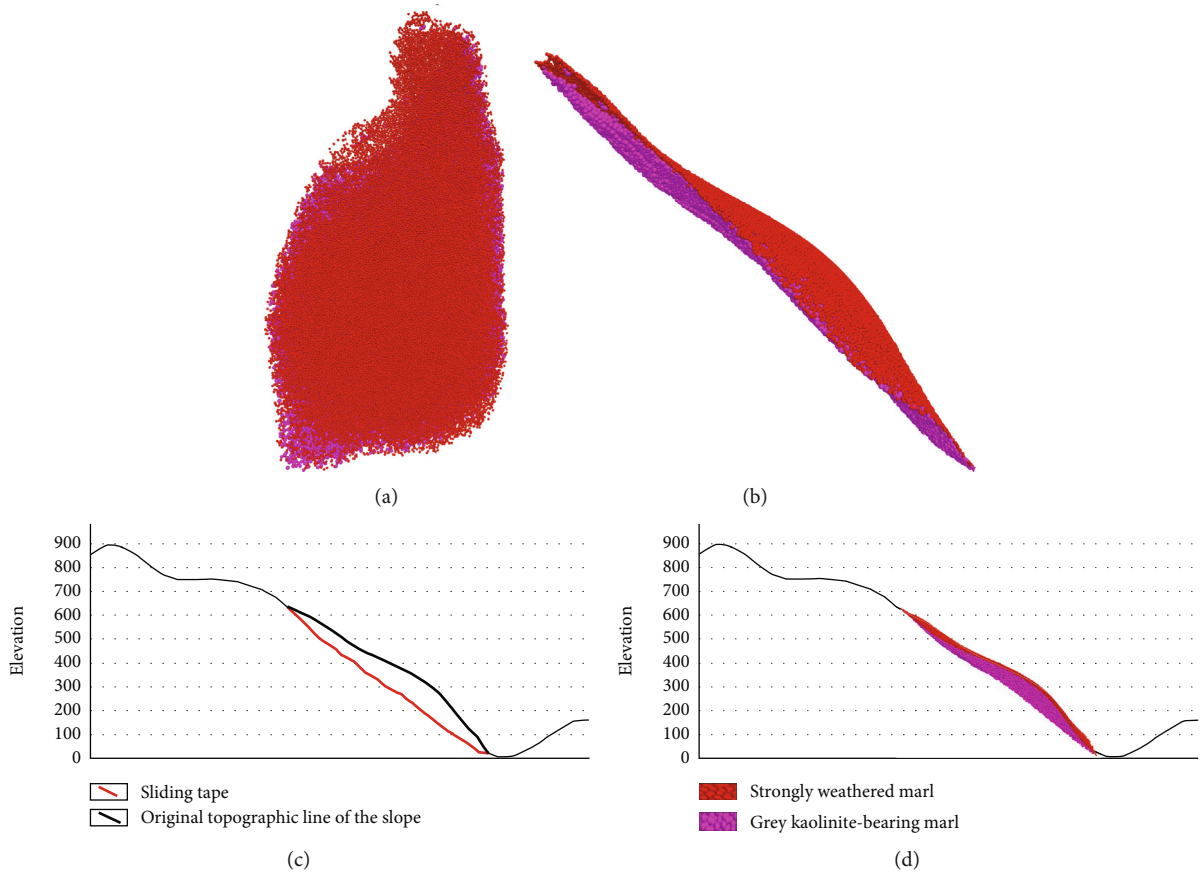

Figure 4: Slip morphology diagram and comparison of model sections. (a) Front view of slip form. (b) Side view of slip form. (c) Presumed preslip and postslip A_1-A_1 profile of the landslide. (d) Numerical model A_1-A_1 profile.

division function to divide the slip bed and slip source area into appropriate triangular grids

(2) Since PFC can only recognize files in DXF and STL formats, the models are exported separately from Rhino in STL format. Using the "geometry import" command, the sliding bed and sliding body triangular mesh models were imported into the PFC as wall boundaries, respectively (Figures 4 and 5). Using the slip wall boundary model as a range, the ball distributes range command was used to generate a reasonable number of particles with specific requirements to fill the slip source area. The gravity is set via the model gravity command to allow the particles to accumulate naturally under gravity

(3) In the early stages of particle generation, due to the large overlap, the time step is set to 1 and the particles are balanced by the model solve command so that the unbalanced forces between the particles are close to 0 (Figure 6).

(4) Assign the parameters in Table 1 to the landslide model and then delete the walls in the slip source area. As the wall's deletion disrupts the particles' original equilibrium, the imbalance of internal stresses can cause many of particles to pop off. At this point, set the particle velocity to zero at a certain time step through the cycle clam command, iterate continuously to obtain the final equilibrium model, and finally make the particle velocity and displacement zero through the ball distribute command. Finally, use the model gravity command to set the gravity

3.4. Monitoring Point Set-up. The purpose of this study is to invert the dynamic process of the Tangjiashan landslide through numerical simulation, monitoring, and recording of the velocity, displacement changes, and trajectories of different parts of the landslide during the whole process of damage-movement-accumulation, which can reflect the movement characteristics of each part of the landslide to a certain extent [8]. The landslide was divided into three parts in the front, middle, and back according to the order of the sliding direction, and a total of 16 monitoring particles numbered 11-16, 5-10, and 1-4 were evenly placed, respectively.

3.5. Selection and Application of Seismic Waves. In this paper, the seismic waves of the Wenchuan earthquake recorded at Wolong station were processed according to the eight magnitude rare earthquakes, and the maximum magnitude of acceleration in the x-direction was 400 cm/s^2, the maximum magnitude of acceleration in the y-direction was 400 cm/s^2, and the maximum magnitude of acceleration

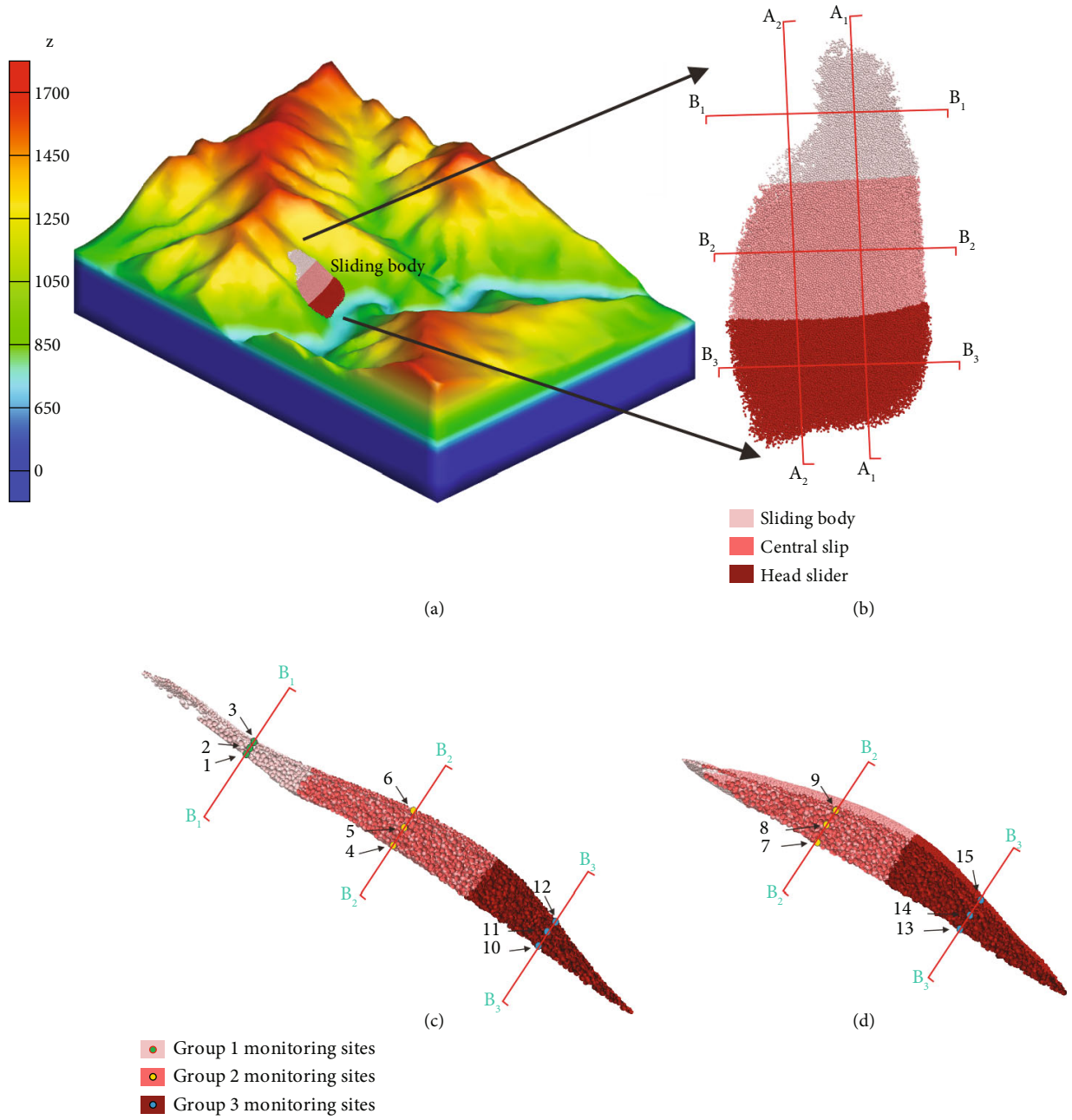

Figure 5: Slip grouping map and distribution of monitoring points. (a) Numerical simulation model diagram. (b) Distribution of slide profile lines. (c) Distribution of monitoring points in profile A_1-A_1. (d) Distribution of monitoring points in profile A_2-A_2.

in the z-direction was 400 cm/s^2, with a dynamic duration of 79 s and a time interval of 0.005 s. The filtered acceleration-time curves are shown in Figure 7, and the first 37 s are selected to be applied to the model in the geographic EW direction, NS, and UD directions, respectively, with a time spacing of 0.01 s, as input to the calculation.

4. Analysis of Slope Damage and Movement Processes

4.1. Dynamic Evolutionary Processes of Landslides. In order to better observe the movement and deformation process of each part of the geotechnical body during the movement of the slide, different parts of the slide were stained and grouped before, during, and after the movement of the slide, and from the comparison of the distribution of the stained and grouped particles at different stages of the slide movement, it was found that the spatial distribution pattern of most of the geotechnical body of the slide did not change significantly (Figure 8).

Based on eyewitness accounts and geological investigations of the site, an analysis of the geological principles shows that the slide body was sliding in the process, except for the rock and soil body at the bottom, which was fragmented by friction during the high-speed sliding process. When the leading edge of the slide came into contact with

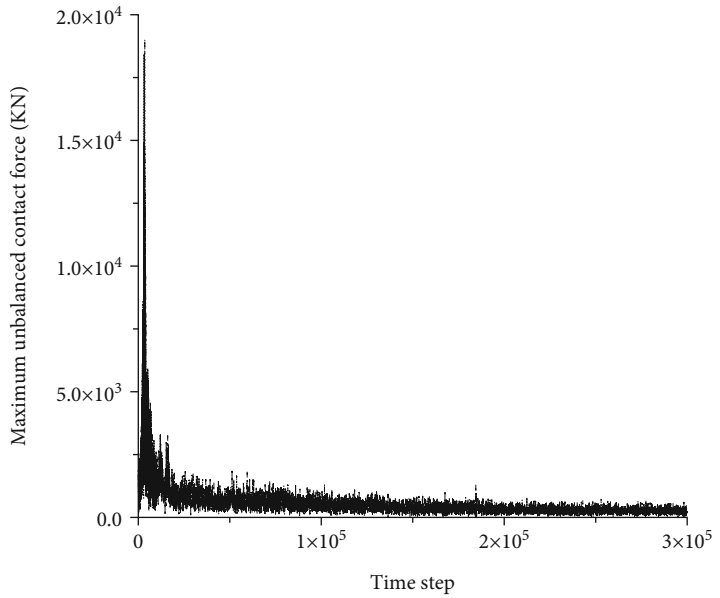

Figure 6: Diagram of maximum unbalance forces during particle equilibrium.

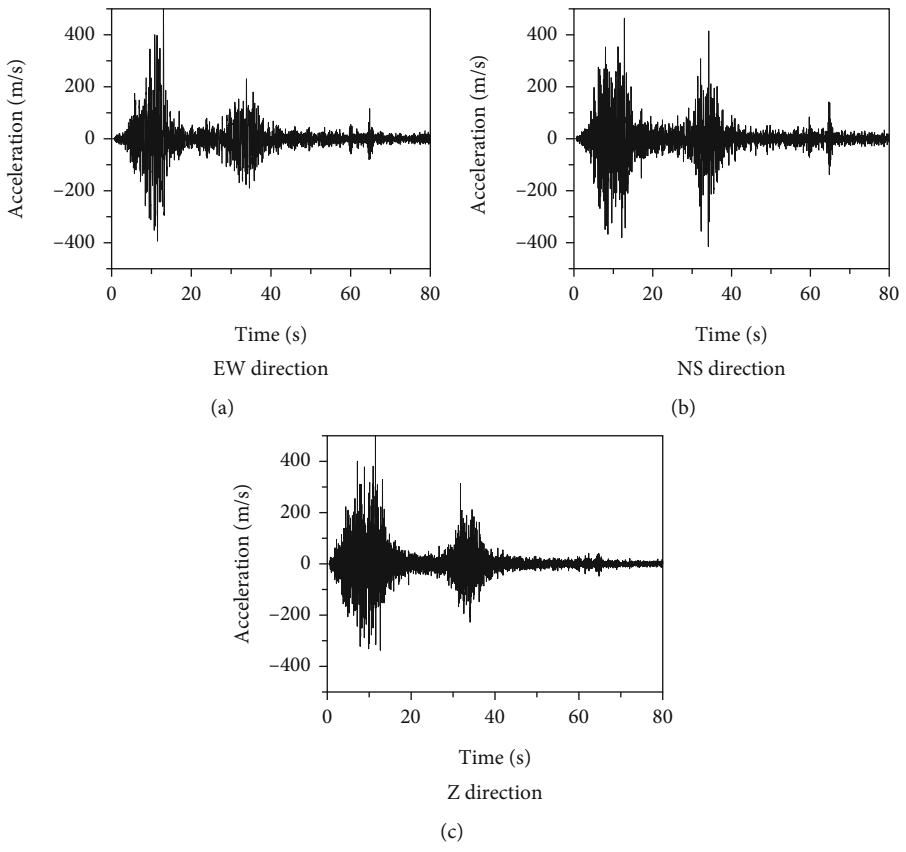

Figure 7: Seismic acceleration time course graph.

the Yuanhe dam on the opposite bank and continued to climb upwards, the vegetation of the Yuanhe dam was cleared away under the action of the scrapers, and the powerful impact also caused the leading edge of the rock and soil body to break up and fall back down (Figure 9), which was eventually thrown on the upper part of the pile.

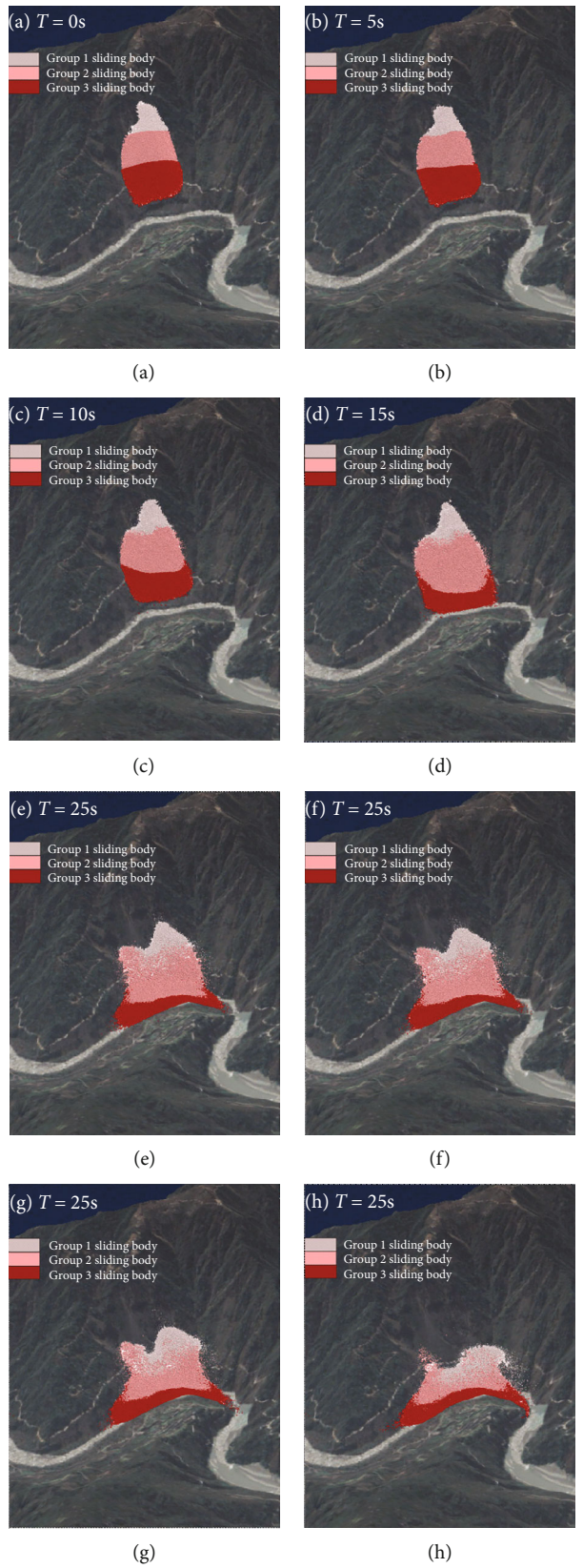

Figure 8: Tangjiashan landslide displacement pattern map.

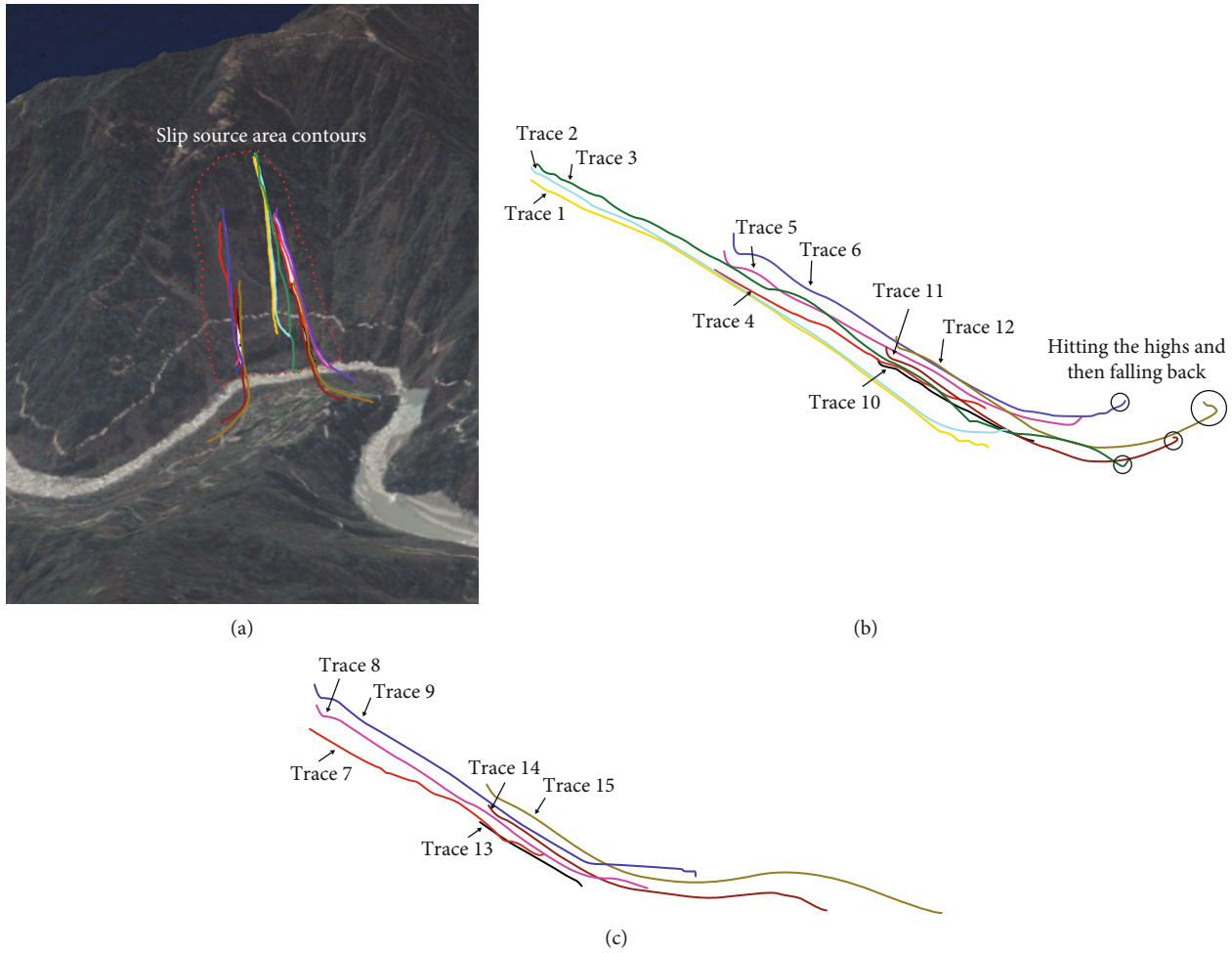

Figure 9: Trajectory monitoring map. (a) Monitoring point trajectory map. (b) A_1-A_1 profile trajectory map. (c) A_2-A_2 profile trajectory map.

Figures 8 and 10 show that the Tangjiashan landslide is divided into four main phases, with the following dynamic processes.

4.1.1. Destabilization and Damage Process of Slopes. The Tangjiashan landslide, in its natural state, produces tensile stress concentration zones and shear stress concentration zones at the shoulder and foot of the slope, respectively, and under the action of tensile stresses, a large number of tensile cracks approximately parallel to the slope surface are produced at the shoulder of the slope. After applying seismic force for 0-5 s, a large number of parallel tensile cracks will develop and extend, forming large tensile cracks through which the slope shoulder debris will roll down to a certain extent. Under the action of wedge splitting, the rock and cracks will continue to make the cracks deeper (Figure 11). The continuous application of seismic forces to pull the cracks continues to extend to the lower part of the slope, causing the locking section to continue to accumulate deformation energy. Based on the site investigation of the landslide, it was found that the slip zone of the Tangjiashan landslide was nearly parallel to the structural surface and belonged to a compliant rocky landslide [27, 28].

4.1.2. The Collapse and Acceleration Phase of the Slide. 5-15 s: the slide continues to accelerate under the action of huge gravitational forces and seismic forces. At about 10 s, the leading edge of the slide first contacts the through-hole channel, and as the direction of the slide's velocity is not in the same plane as the ground plane of the channel, the slide has to continue to slide forward, the channel produces a huge resistance to the slide, and the trend of increasing velocity of the front slide slows down sharply. The first peak of the seismic force also occurred at about 10 s. Although the movement of the front slide was blocked at this point and resistance was transmitted to the middle and rear slide, the trend of increasing velocity of the middle and rear slide did not change significantly under the combined effect of the first peak of the seismic force and the resistance transmitted by the lower slide. At the 10-15 s stage, the leading edge of the slip body had crossed the entire river channel from the Tongkou riverside and touched the foot of the Yuanhe dam on the opposite side. During this process, the front slide should have decreased in speed as the direction of movement was forcibly changed. However, at about 10 s, the speed of the middle and rear slide had already exceeded that of the front slide, so the front slide would have been

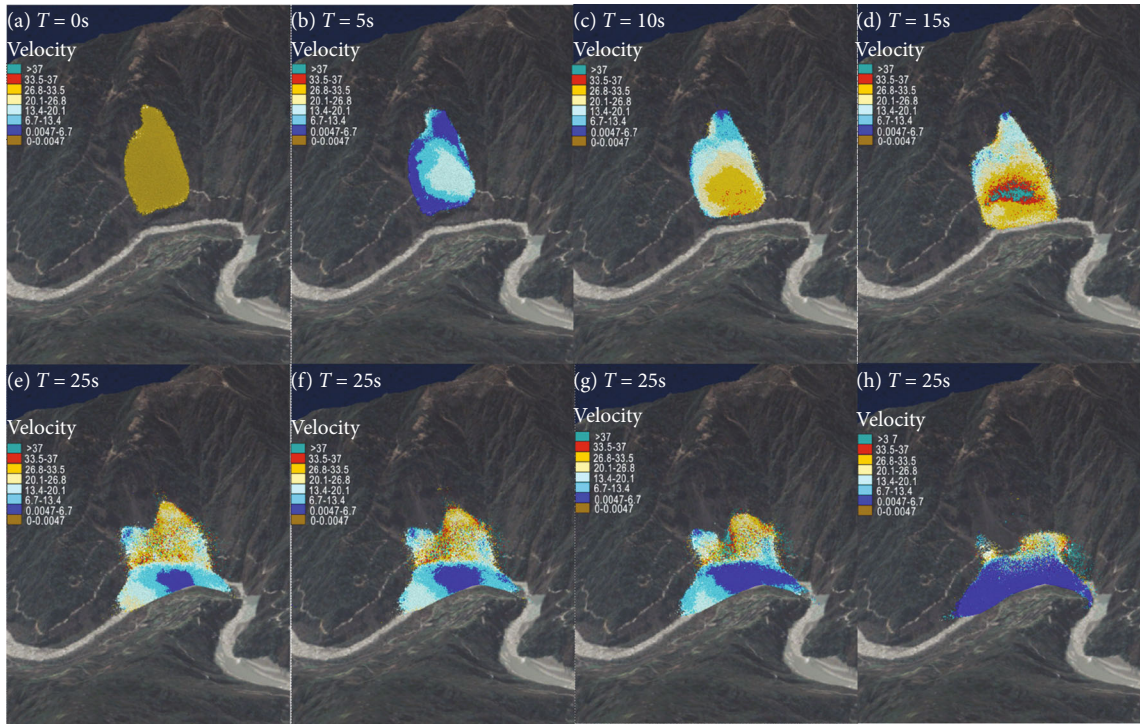

Figure 10: Simulation of the velocity movement of the Tangjiashan landslide.

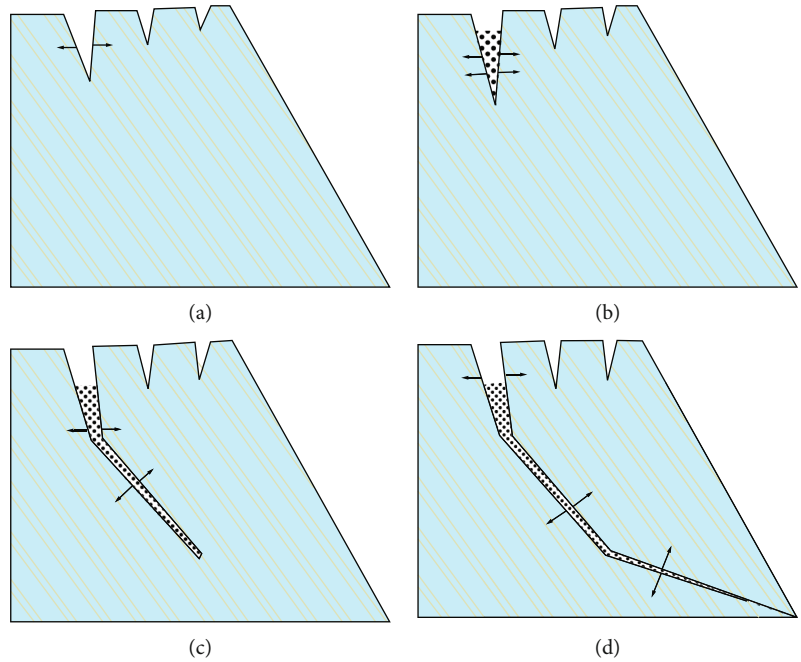

Figure 11: Schematic diagram of pull-apart landslide damage [28]. (a) Severe seismic forces have caused tension cracks in the shoulders of slopes. (b) As the tension cracks expand, debris from the top of the slope rolls into them. (c) Further extension of tension cracks and accumulation of deformation energy in the locking section. (d) The locking section is sheared off, the slope is unstable and the landslide is initiated.

pushed by the slide behind it to maintain its trend of increasing speed. Until about 15 s, when the front edge of the slide touched the Yuanhe dam, and the leading edge of the slide encountered the most violent blockage, with the leading edge continuing to impact upwards into the Yuanhe dam, the acceleration phase ends. The velocity of the leading slip decreases dramatically until it reaches zero.

4.1.3. High-Speed Movement Phase of the Sliding Body. 15-25 s: the slide body enters the high-speed sliding phase. During the

Table 2: Monitoring results for distance and speed of movement at monitoring points.

Group	Location	Distance travelled (m)			Peak speed ($m.s^{-1}$)		
		Maximum	Minimum	Average	Maximum	Minimum	Average
1	Slip head	499.37	155.73	347.36	35.71	12.79	25.43
2	Middle of the slide	567.15	320.17	460.11	41.88	29.49	35.55
3	Slip tail	700.07	646.17	667.41	53.36	40.97	45.42
4	Slip surface	700.07	410.15	535.48	53.36	31.29	39.86
5	Slip mid-level	655.84	375.56	482.86	41.96	26.04	34.03
6	Lower slip	646.17	155.732	351.03	40.97	12.79	26.46

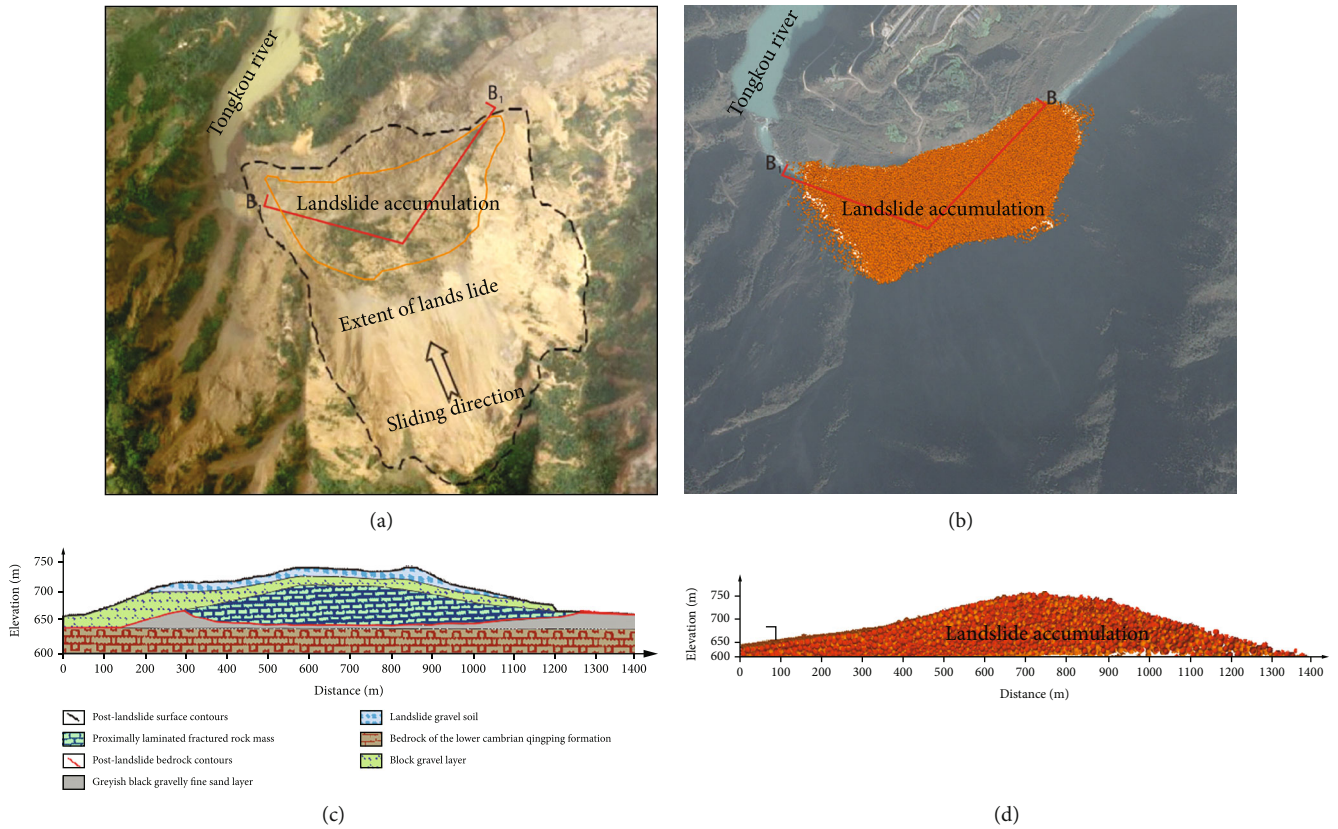

Figure 12: Comparison of landslide accumulations [29]. (a) Postlandslide satellite imagery. (b) Numerical simulation of the top view of the stack. (c) Geological section of the weir B_1-B_1 section. (d) Weir body b-b profile.

acceleration phase, the parallel bond is gradually broken, indicating that the slide body has gradually disintegrated during this phase. When the slide enters the high-speed stage, the parallel bond is almost completely broken, and due to the extremely high sliding speed, the underlying rock and soil bodies collides with the slide bed, causing some of the rock and soil body to be severely fragmented. There is a large amount of fragmented rock and soil mixed with air and water at the base of the slide, and the complex interaction has combined to form a fluid-like mixture, which significantly reduces the friction coefficient between the slide and the slide bed and promotes the high-speed movement of the slide. This resulted in the mid and posterior slides being in contact with the bottom of the Tongkou river channel, where the direction of movement was drastically altered, with the trend of increasing velocity being barely affected and reaching a peak velocity of 39.89 m/s.

4.1.4. Deceleration and Build-up Phase of the Slide. 25-37 s: as the river has been filled with a weir filled with the front slip, the coefficient of friction on its surface is much greater than that of the wet river, the central slip is greatly impeded, and its velocity decreases sharply. As the upper slide body occupies too little mass, although the upper slide body speed is still increasing, it also defines this stage as the deceleration stage. At this time, the front and middle slides have moved to Tongkou river, although it is continuing to move, the speed is very low, almost zero. During the 25-30 s phase, the rear slide was still sliding in the slide bed and encountered the second wave of seismic force, so although the

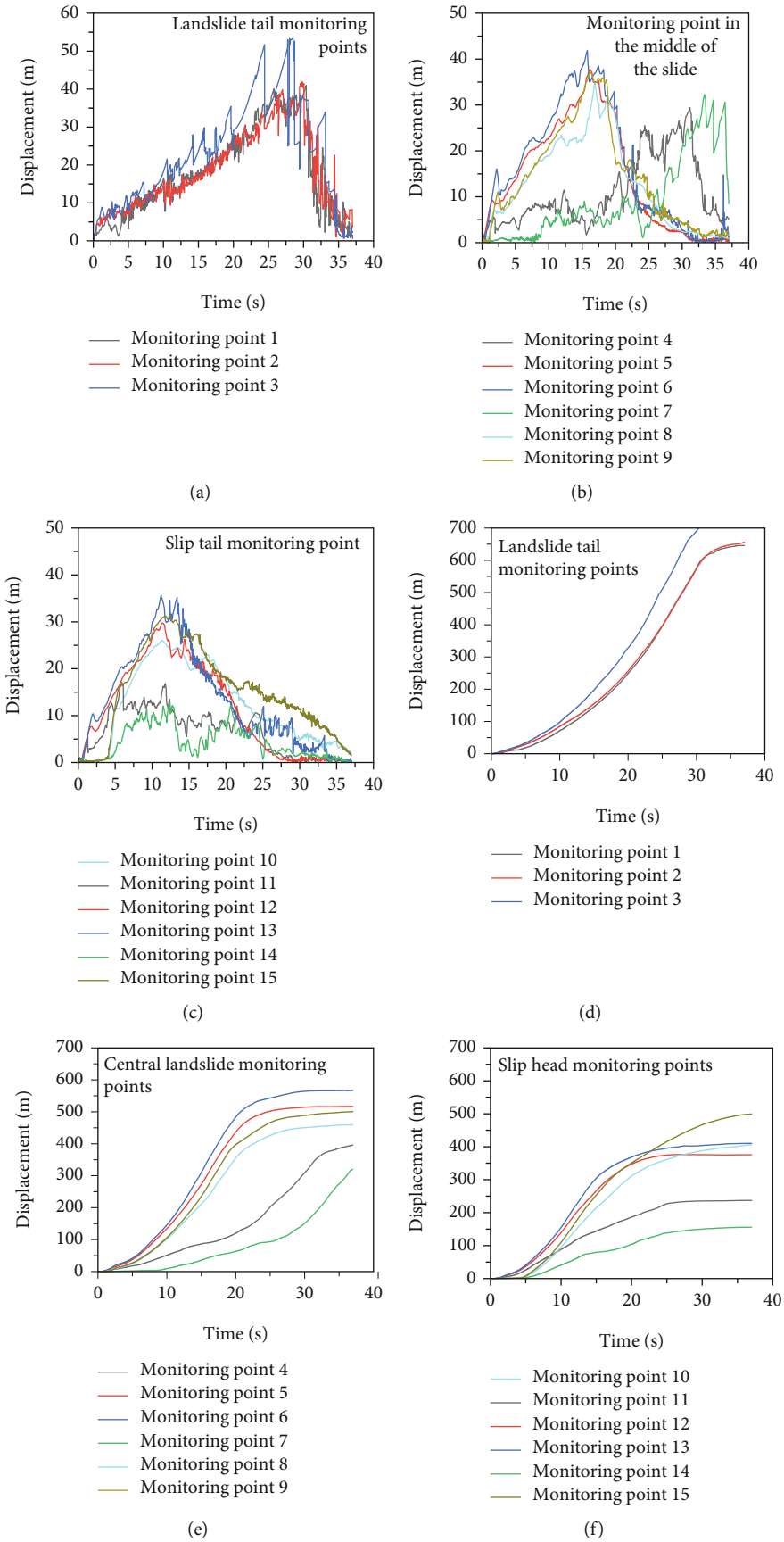

Figure 13: Comparison of velocity displacement at head, middle, and tail monitoring points.

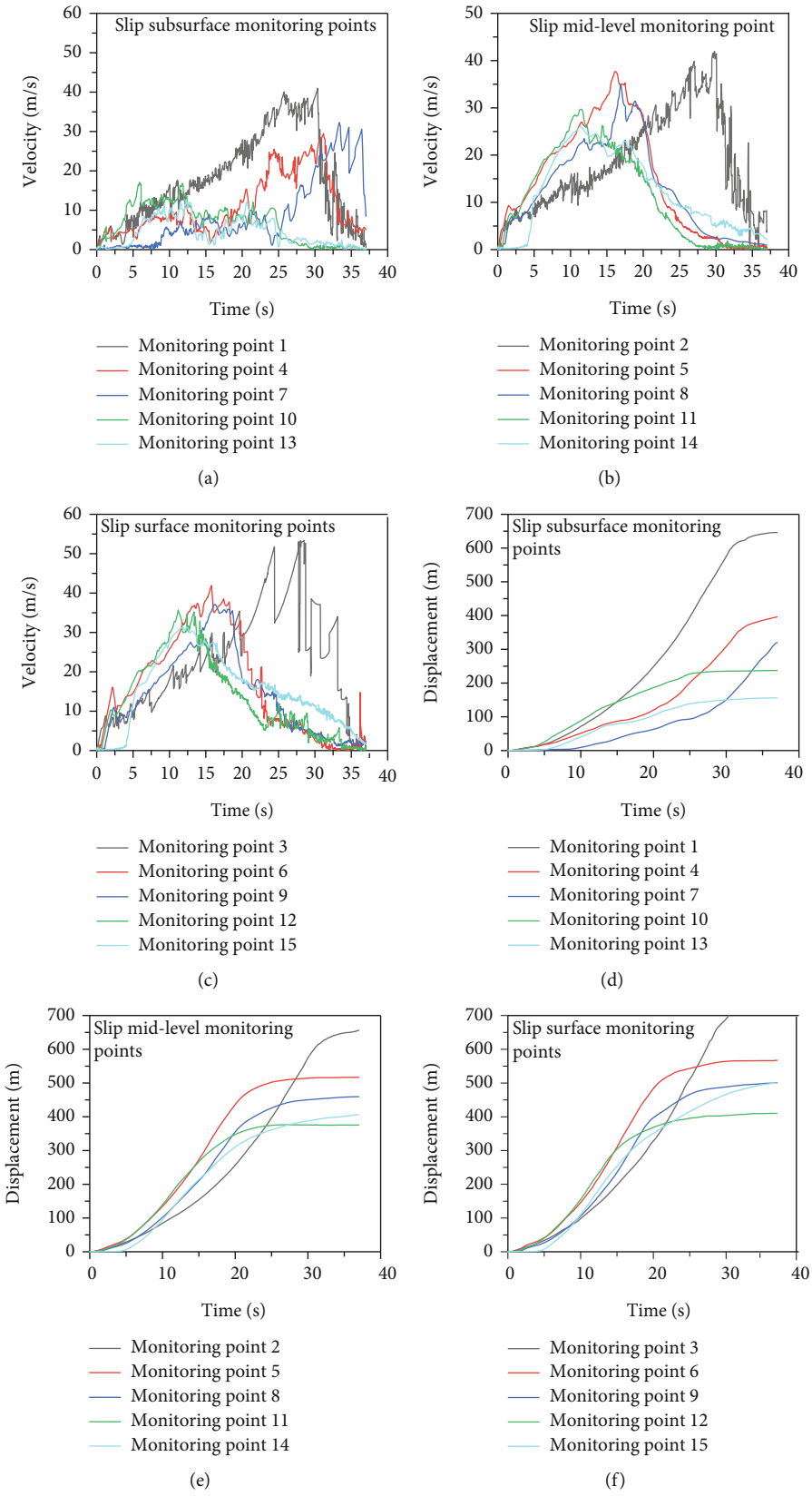

Figure 14: Comparison of velocity displacements at surface, middle, and lower monitoring points.

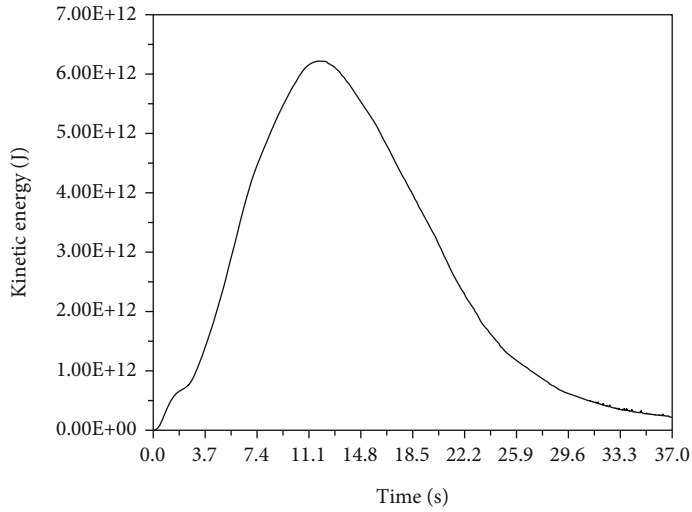

Figure 15: Slip kinetic energy time curve.

central slide blocked the rear slide, the trend of increasing velocity was hardly changed under the added effect of the second wave of seismic force. Until about 30 s, when most of the rear slide impacted and covered the central slide, the slide movement was directly blocked, and the acceleration phase ended with a peak velocity of 41.96 m/s, which was also the maximum velocity of the monitored slides (Table 2). 30-37 s: all parts of the slides had very low velocities and were part of the stacking step break, with most of the slides going to zero velocity and only a small number of slides still moving at low velocities (Figure 11).

4.2. Characterization and Morphological Analysis of the Mound. At 37 s, the velocity of the landslide's front, middle, and rear parts are almost zero, and the accumulation is basically completed. According to the simulation analysis of the dynamic process of the landslide, the maximum width of the landslide source area is about 100 m, and the plane projection area is about 1500 m^2, with an overall lap-chair shape. As the leading edge of the landslide is blocked from sliding when it touches the Yuanhe dam, the speed of the leading edge decreases sharply and also gives a strong resistance to the central as well as the rear slide, the slide starts to expand to both sides, and the width of the slide becomes larger, up to which the overall shape of the slide starts to change significantly. The length of the landslide mound is about 800 m along the river, the maximum width across the river is about 600 m, the plane area is about 300,000 m^2, the height of the dam is 82-124 m, and the volume is about 20 million m^3, the overall fan-shaped distribution (Figure 10 and Figure 12). The top of the weir is about 300 m wide, and the overall topography is undulating, showing a topographic distribution along the river crossing direction, with the middle and front part being higher, the middle and back part being the next highest, and the middle part being the lowest. The mounding features obtained from the simulation analysis (Figure 12(b)and Figure 12(d)) are all consistent with the actual mounding features (Figure 12(a) and Figure 12(c)).

4.3. Velocity and Trace Analysis. As shown in Figure 6, in order to monitor the characteristics of the velocity, displacement, and movement trajectory of the landslide at different times, three groups of 15 monitoring particles were set up in the landslide particle model, which are No. 1-3 in the rear of the landslide, No. 4-10 in the middle. and No. 11-15 in the front.

The particles' trajectory reflects the sliding-accumulation process of the Tangjiashan landslide. It can be seen that the front slide of the Tangjiashan landslide shows a tendency to spread to both sides, while the middle and rear slide show a nearly straight line movement (Figure 9), mainly because the front slide hits the Yuanhe dam directly and is subject to the strongest squeezing effect itself, while the middle and rear slide barely hits the Yuanhe dam and consumes its kinetic energy in the process of friction with the front slide. The kinetic energy is used up in friction with the front body [27].

From the velocity and time characteristics of the monitored particles, it can be seen that the front slide has the fastest velocity growth, the shortest growth process duration, the smallest velocity peak, the shortest descent duration, and the smallest final displacement. The rear sliding body has the slowest velocity growth, the longest growth process duration, the largest velocity peak, the longest descent duration, and the largest final displacement (Figures 13 and 14). This is mainly because the front slide displacement is the shortest (Table 2), the acceleration distance is short, and the middle and rear slide acceleration distance is longer. And the rear slide acceleration time is long enough to catch the second peak of the seismic force, about 20 s at the dividing line, the second acceleration phenomenon is obvious, the central and front slide is not this phenomenon. In addition, although the front body directly impacted the Yuanhe dam, the process of impacting the Yuanhe dam due to the scraping action will greatly reduce the friction; the middle body in the slide into the Tongkou river is overlaid on the upper layer of the front body, so it is greater than the sliding friction of the wet riverbed; the upper body in the slide into

the Tongkou river, due to its small mass, inertia is small, once it encounters the bump not yet fully completed stacking is enough to make it lose most of the slide. Body is divided according to the surface, middle and lower layers, and it can be found that the speed and distance of movement of the slide body show a trend of decreasing speed from the surface layer to the bottom layer at any moment of the landslide (Table 2), which eventually also leads to decreasing displacement. Based on the results of the engineering site investigations and the displacement and velocity-time curves from the numerical simulations, it can be assumed that the controlling factor for the maximum velocity of the Tangjiashan landslide is the slip distance.

The kinetic energy time curve and the velocity time curve of the slide (Figures 14 and 15) show that the peak of the overall kinetic energy and the peak velocity of the mid-level slide correspond to each other occurring at about 15 s. This phenomenon also confirms that the middle slip is indeed the main mass component of the slip. It is worth noting that the surface slide, although not a major reference factor in the description of landslide movement, exhibits characteristics distinctly different from those of the other parts of the slide (Figures 13 and 14). As can be seen in Table 2, the surface slide is much higher than the other parts of the slide in terms of both velocity and displacement and exhibits distinct debris flow characteristics.

5. Conclusion

In this paper, the macroscopic and fine-scale mechanical parameters of the sliding body were determined based on indoor mechanical tests and discrete element numerical simulations. Combined with topographical features and accumulation characteristics of the landslide, the ultra-large compliant rocky landslide of the Tangjiashan landslide is taken as the research object. Based on the high-precision Dem data and pre- and postlandslide image data, a 3D landslide model was established. The complete dynamic process of the Tangjiashan landslide was inverted using the numerical simulation program PFC3D and the characteristic data on the velocity, displacement, and morphology of the landslide body was monitored and analysed. The following conclusions were obtained:

(1) The main slide direction of the Tangjiashan landslide is NW160°, and its dynamic evolution process can be divided into four stages: destabilisation and destruction, collapse and accelerated sliding, high speed sliding, and decelerating accumulation. The maximum sliding distance is about 642.05 m and the maximum sliding speed is about 38.67 m/s, which is a typical high-speed short-range landslide

(2) Under the action of strong seismic forces, the slope first undergoes traction damage and then slides towards the Tongkou river. Under the coupling effect of seismic force and gravity, the sliding velocity also grew until it struck the Yuanhe dam on the opposite side, and almost simultaneously the rear slide reached a maximum velocity of 38.67 m/s. Thereafter, most of the slide motion stopped sharply, but a small number of slides at the leading edge remained in motion and continued to impact upwards along the Yuanhe dam until the kinetic energy was exhausted before falling back down. By monitoring the trajectory of the leading edge slides, it can be found that there is indeed an obvious rush up and back down phenomenon

(3) Using the numerical simulation program PFC3D, the complete sliding process of the Tangjiashan landslide was reproduced, and the results matched well with the actual investigation. The results show that the destabilisation process of the Tangjiashan landslide lasts about 5 s, the acceleration phase lasts about 10 s, the high speed phase lasts about 10 s and the deceleration and accumulation phase lasts about 12 s. The whole process lasts about 37 s. During the sliding process, the structural integrity of most of the landslide is well preserved, except for the leading edge of the landslide, which is broken and dispersed due to the impact on Yuanhe dam

(4) Tangjiashan is a traction landslide, which is divided according to the front middle and back along the main slide direction. And the rear back slide has the characteristics of large slide distance, slow velocity growth, high maximum velocity, and fast velocity drop. The landslide is divided into the surface, middle, and bottom layers. And the landslide movement velocity shows a trend of gradually decreasing from the surface to the bottom layer. The velocity of the surface slide is much higher than that of the other parts, which shows obvious detrital flow characteristics. In the Tangjiashan landslide, the slip distance is the controlling factor for the landslide velocity in different parts

(5) Based on the high-precision Dem data, the use of Rhino can quickly and accurately build a three-dimensional model of the landslide. And it is in good conformity with the actual topography of the landslide, which can meet the needs of the numerical simulation of PFC3D

Data Availability

The data used to support the findings of this study are included within the article.

Conflicts of Interest

The authors declare that they have no conflicts of interest.

Acknowledgments

This work was supported by the National Natural Science Foundation of China (41772163).

References

[1] H. U. Xiaobo, F. A. N. Xiaoyi, and T. A. N. G. Junjie, "Accumulation characteristics and energy conversion of high-speed and long-distance landslide on the basis of DEM: a case study of Sanxicun landslide," *Journal of Geomechanics*, vol. 25, no. 4, pp. 527–535, 2019.

[2] T. Huang, M. T. Ding, T. She, S. J. Tian, and J. T. Yang, "Numerical simulation of a high-speed landslide in Chenjiaba, Beichuan China," *Journal of Mountain of Science : English*, vol. 14, no. 11, p. 13, 2017.

[3] S. Y. Ma, C. Xu, X. W. Xu et al., "Characteristics and causes of the landslide on July 23, 2019 in Shuicheng, Guizhou Province, China," *Landslides*, vol. 17, no. 6, pp. 1441–1452, 2020.

[4] Z. Y. Cai, E. L. Liu, N. S. Chen, J. L. Feng, G. S. Hu, and Y. Su, "Numerical analysis of the initiation and sliding process of the Yigong landslide using a continuous-discontinuous method," *Environmental Earth Sciences*, vol. 18, no. 5, 2022.

[5] Y. X. Song, D. Huang, and D. F. Cen, "Numerical modelling of the 2008 Wenchuan earthquake-triggered Daguangbao landslide using a velocity and displacement dependent friction law," *Engineering Geology*, vol. 215, pp. 50–68, 2016.

[6] W. H. Zhao, X. L. Xia, X. L. Su, Q. H. Liang, X. W. Liu, and N. P. Ju, "Movement process analysis of the high-speed long-runout Shuicheng landslide over 3-D complex terrain using a depth-averaged numerical model," *Landslides*, vol. 181, pp. 1–14, 2021.

[7] C.-M. Lo, C.-F. Lee, and W.-K. Huang, "Failure mechanism analysis of rainfall-induced landslide at Pingguang stream in Taiwan: mapping, investigation, and numerical simulation," *Environmental Earth Sciences*, vol. 75, no. 21, pp. 1–6, 2016.

[8] C. Shi, D.-j. Li, K.-h. Chen, and J.-w. Zhou, "Failure mechanism and stability analysis of the Zhenggang landslide in Yunnan Province of China using 3D Particle Flow code simulation," *Journal of Mountain Science*, vol. 13, no. 5, pp. 891–905, 2016.

[9] C. L. Tang, J. C. Hu, M. L. Lin et al., "The Tsaoling landslide triggered by the Chi-Chi earthquake. Taiwan: insights from a discrete element simulation," *Engineering Geology*, vol. 106, no. 1-2, pp. 1–19, 2009.

[10] R. Poisel and A. Preh, "3D landslide run out modelling using the Particle Flow Code PFC3D," in *Landslides and Engineered Slopes. From the Past to the Future*, pp. 873–879, CRC Press, 2008.

[11] C. M. Lo, M. L. Lin, C. L. Tang, and J. C. Hu, "A kinematic model of the Hsiaolin landslide calibrated to the morphology of the landslide deposit," *Engineering Geology*, vol. 123, no. 1-2, pp. 22–39, 2011.

[12] A. Ray, H. Verma, A. K. Bharati, R. Rai, R. Koner, and T. N. Singh, "Numerical modelling of rheological properties of landslide debris," *Natural Hazards*, vol. 110, no. 3, pp. 2303–2327, 2022.

[13] X. Chen, Z. Zhao, J. B. Wei, and C. Xu, "Numerical study of Mabian landslide kinematics and impact intensity," *Coalfield Geology and Exploration*, vol. 49, no. 4, pp. 234–241, 2021.

[14] Z. X. Zou, H. M. Tang, C. R. Xiong, A. J. Su, and R. E. Criss, "Kinetic characteristics of debris flows as exemplified by field investigations and discrete element simulation of the catastrophic Jiweishan rockslide, China," *Geomorphology*, vol. 295, pp. 1–15, 2017.

[15] J. W. Zhou, P. Cui, and H. Fang, "Dynamic process analysis for the formation of Yangjiagou landslide-dammed lake triggered by the Wenchuan earthquake, China," *Landslides*, vol. 10, no. 3, pp. 331–342, 2013.

[16] Y. Y. Wu, M. Zhang, L. Yang et al., "Failure mechanisms and dynamics of the Shanzao rockslide in Yongjia County, China on 10 august 2019," *Landslides*, vol. 18, no. 7, pp. 2565–2574, 2021.

[17] X. D. Chen and H. F. Wang, "Slope failure of noncohesive media modelled with the combined finite-discrete element method," *Applied Sciences*, vol. 9, no. 3, p. 579, 2019.

[18] Z. L. Zhang, T. Wang, S. S. Wu, H. M. Tang, and C. Y. Liang, "The role of seismic triggering in a deep-seated mudstone landslide, China: historical reconstruction and mechanism analysis," *Engineering Geology*, vol. 226, pp. 122–135, 2017.

[19] W. J. Xu, Q. Xu, and Y. J. Wang, "The mechanism of high-speed motion and damming of the Tangjiashan landslide," *Engineering Geology*, vol. 157, pp. 8–20, 2013.

[20] Y. Huang, W. J. Zhang, Q. Xu, P. Xie, and L. Hao, "Run-out analysis of flow-like landslides triggered by the Ms 8.0 2008 Wenchuan earthquake using smoothed particle hydrodynamics," *Landslides*, vol. 9, no. 2, pp. 275–283, 2012.

[21] Q. M. Zhong, S. S. Chen, S. A. Mei, and W. Cao, "Numerical simulation of landslide dam breaching due to overtopping," *Landslides*, vol. 15, no. 6, pp. 1183–1192, 2018.

[22] Y. Zhu, M. Peng, S. Cai, and L. Zhang, "risk-based warning decision making of cascade breaching of the Tangjiashan landslide dam and two smaller downstream landslide dams," *Frontiers in Earth Science*, vol. 9, p. 648919, 2021.

[23] L. Wang, X. Zhang, F. Zaniboni, E. Onate, and S. Tinti, "Mathematical optimization problems for particle finite element analysis applied to 2D landslide modeling," *Mathematical Geosciences*, vol. 53, no. 1, pp. 81–103, 2020.

[24] Z. S. Zheng, S. A. Wang, S. Zheng, and X. H. Qu, "Numerical simulation of particle flow for high velocity compaction based on discrete element method," *Rare Metal Materials and Engineering*, vol. 39, no. 12, pp. 2132–2136, 2010.

[25] E. Eberhardt, D. Stead, and J. S. Coggan, "Numerical analysis of initiation and progressive failure in natural rock slopes–the 1991 Randa rockslide," *International Journal of Rock Mechanics and Mining Sciences*, vol. 41, no. 1, pp. 69–87, 2004.

[26] W. Cao, W. Z. Li, B. Tang, G. Deng, and J. F. Li, "PFC study on building of 2D and 3D landslide models," *Journal of Engineering Geology*, vol. 25, no. 2, pp. 455–462, 2017.

[27] Y. J. Bao, Y. Huang, and G. R. Liu, "SPH simulation of high-volume rapid landslides triggered by earthquakes based on a unified part II: solid-liquid-like phase transition and flow-like landslides," *International Journal of Computational Methods*, vol. 17, no. 4, 2020.

[28] R. L. Liu, Y. H. Han, J. Xiao, and T. Wang, "Failure mechanism of TRSS mode in landslides induced by earthquake," *Scientific Reports*, vol. 10, no. 1, p. 21326, 2020.

[29] B. Wang, S. Yang, and C. Chen, "Landslide dam breaching and outburst floods: a numerical model and its application," *Journal of Hydrology*, vol. 609, p. 127733, 2022.